Remotely Addressable Magnetic Composite Micropumps†

Eric Diller, Shuhei Miyashita, and Metin Sitti*

Received Xth XXXXXXXXXX 20XX, Accepted Xth XXXXXXXXX 20XX
First published on the web Xth XXXXXXXXXX 20XX
DOI: 10.1039/b000000x

Remotely and selectively turning on and off the magnetization of many micro-scale magnetic actuators could be a great enabling feature in fields such as microrobotics and microfluidics. We present an array of addressable $800 \times 800 \times 75\,\mu\text{m}^3$ micropumps made from a composite material whose net magnetic moment can be selectively turned on or off by application of a large magnetic field pulse. The material is made from a mixture of micron-scale Neodymium-Iron-Boron and Ferrite particles, and can be formed into arbitrary actuator shapes using a simple molding procedure. By selectively controlling the orientation of each of an array of micro-actuators prior to the application of the field pulse, the magnetic on/off state of each can be controlled independently. The micropumps are actuated by rotating magnetic fields up to $12\,\text{kA m}^{-1}$ in strength to pump liquid through $100\,\mu$m fluid channels. A distinct transition between the on and off states is seen by application of pulsed magnetic fields of about $240\,\text{kA m}^{-1}$ in strength. As a demonstration, we show addressable on/off control of two micropumps and five simple spinning magnetic microactuators, with potential applications for lab-on-a-chip type fluidic devices.

1 Introduction

Recent works in micro-scale magnetic actuation have enabled the creation of micron-scale permanent magnets for the application of forces and torques via externally-generated magnetic fields for microfluidic pumps and mixers,[1,2] mobile microrobots[3–6] and other microdevices.[7,8] One common goal has been the parallel actuation of many microdevices.[6] To effectively use many devices, independent addressing of these devices has been attempted,[9–12] but all presented methods have major limitations in performance or number of addressable devices. The ability to remotely and repeatedly turn on and off magnetic microdevices is an unsolved problem which could be used to independently address multiple devices which share the same workspace in enclosed environments such as in microfluidic channels in lab-on-a-chip devices. Therefore, this study aims to develop a method to remotely turn microdevices on and off in an addressable manner.

We propose micro-scale permanent magnet composites that can be remotely and reversibly turned on and off by the application of a pulsed magnetic field along the magnetic axis, supplied by electromagnetic coils outside the device operation workspace. This concept is similar to *electropermanent magnets*, which pair switchable permanent magnets with electromagnets. In these devices, electromagnetic coils are wrapped directly around some of an array of switchable permanent magnets. When a strong current is pulsed through the coils, the magnetization of some of the permanent magnets is switched, allowing for an on-off behavior of the set. These devices were originally developed as centimeter-scale or larger magnetic workpiece holders.[13] While millimeter-scale *electropermanent magnets* have been fabricated,[14] they contain integrated switching coils, preventing their scaling down to the micrometer scale for untethered operation. The magnetic composite material proposed in this paper can be scaled down to the micron-scale and enables remote wireless control. The anisotropic composite is made from two materials of equal magnetic moment: one permanent magnet material of high coercivity and one material which switches magnetization direction by applied fields. By switching the second material's magnetization direction, the two magnets either work together or cancel each other, resulting in distinct on and off behavior of the device. The device can be switched on or off remotely using a field pulse of short duration. Because the switching field pulse covers the entire workspace, this method can be used to selectively disable and enable many microdevices concurrently based on their orientations. Orientation control is achieved by a multi-step process using a field gradient to select a device for disabling by controlling each device's orientation.

As a demonstration of this remotely addressable actuation method for potential lab-on-a-chip applications, we present an array of micropumps which can be selectively disabled for on/off pumping of liquids through microchannels. We show the addressable control of two micropumps and five simple spinning magnetic actuators to demonstrate the scalability of the method. Micropumping is a critical element in many microfluidic systems,[15] and so offers a relevant application of

† Electronic Supplementary Information (ESI) available: [Videos of selective disabling of two micropumps and five microdevices are given]. See DOI: 10.1039/b000000x/

5000 Forbes Ave., 320 Scaife Hall, Pittsburgh, PA 15213, USA. Fax: 412 268 3348; Tel: 412-268-3632; E-mail: sitti@cmu.edu

the disabling magnetic actuation. The micropump design presented here is used to simply demonstrate the magnetic disabling concept, so a study of the pumping performance is beyond the scope of this work. As the micropumps are fabricated using a simple molding process, this addressable actuation method could be applicable for any micro-scale magnetic actuator used in microfluidic channels or microrobotics.

2 Experimental methods

2.1 Magnetic actuation

Micropump motion actuation is achieved by rotating magnetic fields which apply magnetic torques to drive the micropump. These fields, up to $\pm 12\,\mathrm{kA\ m^{-1}}$ in strength, are provided by three air-core electromagnetic coil pairs, which can create a uniform field in any direction in the workspace, as presented previously.[16] The coils and workspace are shown in Fig. 1(a). The currents in the electromagnetic coils are controlled using a PC with data acquisition system using linear electronic amplifiers (Dimension Engineering Inc., SyRen 25) and Hall-effect current sensors (Allegro Microsystems Inc., ACS714). Imaging of the workspace is accomplished by a CCD camera (Foculus). The magnetization switching field pulse H_{pulse} is created with a 20-turn, low-inductance (8 mH) coil of inner diameter 23 mm, placed inside the larger motion actuation coils as shown in Fig. 1(a). The pulsing coil is driven by a 0.8 mF electrolytic capacitor bank in an LCR circuit, switched by silicon-controlled rectifier (Vishay, VS-70TPS12), delivering a peak current of around 450 A. The resulting H_{pulse} is measured with a Hall effect sensor (Allegro 1321), and shown as a function of time in Fig. 1(b) for a 130 V capacitor charge. The pulse lasts several milliseconds, with peak amplitude linearly proportional to the capacitor charge voltage. Because the magnetic microdevice is free to rotate, it tends to align with an applied field, which would prevent a disabling pulse from being effective. However, for a relatively fast pulse, the device inertia, fluid drag and surface friction act to keep it from aligning with the field. The approximately 100 μs H_{pulse} rise-time switches the device completely before it orients to the field, as discussed in section 3.1. The workspace, which is located inside both sets of coils, contains the microdevices and fluid channels, where the devices rest. The fluid used is viscous silicone oil (Dow Corning, 5-20 cSt), which eases the disabing process by increasing the viscous drag torque on the micropump.

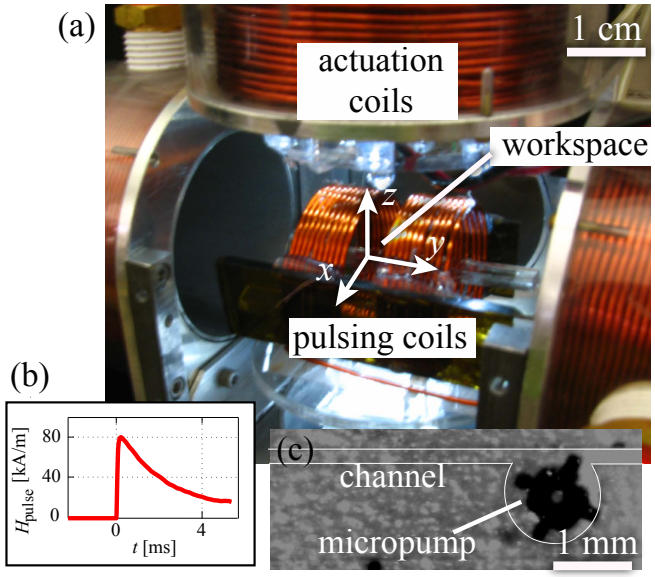

Fig. 1 Photograph of the electromagnetic coil system: (a) Actuation and pulsing coils surrounding the workspace; (b) Measured H_{pulse} as a function of time for a 130 V capacitor charge, showing a peak of $240\,\mathrm{kA\ m^{-1}}$ and duration of several milliseconds; (c) The micropump and channel used in this study.

2.2 Powder composite magnetization disabling

2.2.1 Magnetic materials. The micropump consists of a microcomposite of two magnetic powders, bound in a non-ferromagnetic polyurethane matrix (BJB Enterprise, TC-892). Neodymium-Iron-Boron (NdFeB, Magnequench MQP-15-7), refined in a ball mill to produce particles under 10 μm in size, is chosen as the high-coercivity material, with measured coercivity of around $600\,\mathrm{kA\ m^{-1}}$. Once magnetized, the NdFeB retains its magnetization direction and magnitude during the experiments. Ferrite ($BaFe_{12}O_{19}$), ground using an end-mill to grains approximately 10-50 μm in size, is chosen as the switching material due to its large remanence and coercivity of around $320\,\mathrm{kA\ m^{-1}}$. This coercivity is larger than the device motion actuation range of $\pm 12\,\mathrm{kA\ m^{-1}}$, but much smaller than the coercivity of NdFeB, allowing for the ferrite to be switched without affecting the NdFeB. Both NdFeB and ferrite can be ground to micrometer size without significant change in magnetic properties. An applied switching field H_{pulse} greater than the coercivity of ferrite, but less than the coercivity of NdFeB, will switch the magnetization of the ferrite. This switching allows the device to be switched between "on" and "off" states as the magnetic moments add or cancel each other. While the internal field of the magnet will not be zero, the net field outside the magnet will be nearly zero in the "off" state, resulting in near zero net magnetic actuation forces and torques.

This type of magnetic disabling cannot be achieved with a single magnetic material. The permeability of magnetic materials is very high when the material is far from saturation, making it difficult to demagnetize a sample exactly with a field pulse. While steadily decreasing AC fields can be used to ef-

fectively demagnetize a magnetic material, this method does not allow for addressable demagnetization because it will disable all magnets in the workspace. Thus, the use of the magnetic composite enables novel untethered addressable magnetic disabling.

2.2.2 Composite magnet fabrication. The magnetic slurry is poured into a rubber mold fabricated using soft-lithography techniques.[17] During curing, the entire mold is placed in a strong uniform magnetic field (800 kA m^{-1}) to induce a preferential "forward" direction and magnetize both magnetic materials. This field orients the individual grains and causes the magnetic particles to form long chain aggregates.[18] This orienting process results in an anisotropic increase in remanent magnetization and coercivity of about 10% in this preferential direction, when compared with a non-oriented sample.

Due to their proximity in the matrix, the magnet grains can potentially interact with each other via exchange coupling, as is the case of exchange spring magnets.[19] If this were the case, the ferrite magnetization would be coupled to the NdFeB, preventing it from switching magnetically and increasing the effective coercivity of the ferrite. However, as the coercivity of ferrite is much higher than the remanence of NdFeB, exchange coupling is considered negligible. This is verified experimentally by noting that the effective observed coercivity of the ferrite is not changed when in composite form with NdFeB.

3 Results

The magnetization H-m loop for the micropump is shown in Fig. 2(a), as taken in an alternating gradient force magnetometer (AGFM, Princeton Measurements MicroMag 2900), with applied field strength up to 1110 kA m^{-1}. The plot shows two distinct saturation moments m_s of about $m_{s,ferrite}$ = 1.5 μA m^2 at 300 kA m^{-1} and $m_{s,ferrite}$ + $m_{s,NdFeB}$ = 3.3 μA m^2 at 800 kA m^{-1}. The moments of the two materials must be equal to cancel exactly when the device is turned off. To allow the fine tuning of this cancellation, the volume ratio of the two materials is chosen so that $m_{s,NdFeB}$ is slightly larger than $m_{s,ferrite}$. The NdFeB magnetizing field is then adjusted in the AGFM in an iterative fashion to lower m_{NdFeB} from its saturation value such that m_{NdFeB} equals $m_{s,ferrite}$.

When fields are applied below the NdFeB coercivity, the NdFeB acts as a permanent magnet, biasing the device magnetization, as shown in the H-m loop of Fig. 2(b) for applied field H_{app} up to ±240 kA m^{-1}. Traversing the hysteresis loop, the device begins in the "off" state at point "A", where motion actuation fields, indicated by the ±12 kA m^{-1} range, only magnetize the device to about 0.08 μA m^2, resulting in minimal motion actuation. To turn the device on, a 240 kA m^{-1} pulse is applied in the forward direction, bringing the device to point "B". After the pulse, the device returns to point "C", in the "on" state. Here, motion actuation fields vary the device moment between about 1.7 and 1.8 μA m^2. To turn the device off, a pulse in the backward direction is applied, traversing point "D", and returning to the "off" state at point "A" at the conclusion of the pulse. For small motion actuation fields in the lateral direction, the device is expected to show even lower permeability in the on or off state due to the shape anisotropy induced during the molding process.

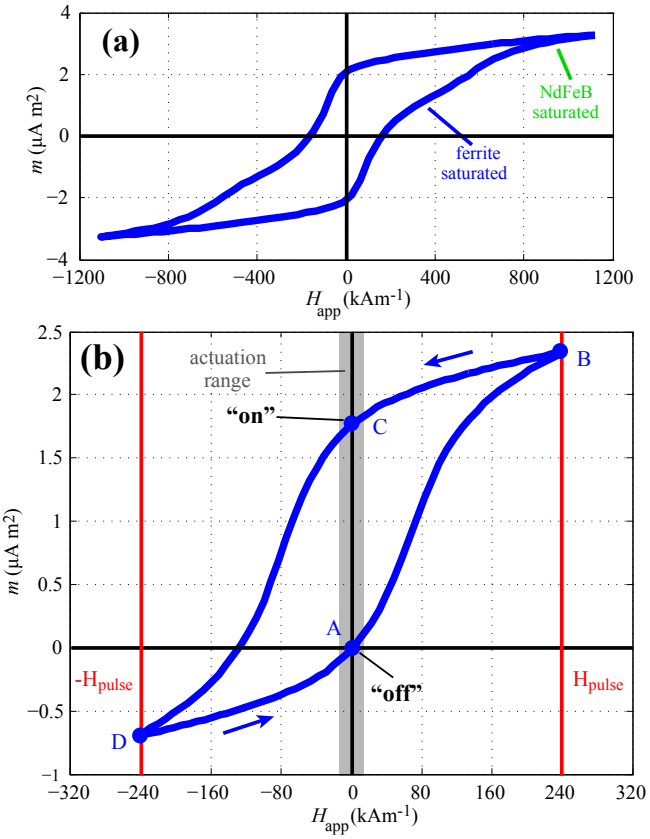

Fig. 2 H-m hysteresis loops of the microdevice, taken in an alternating gradient force magnetometer. (a) The microdevice magnetic moment for applied field up to 1110 kA m^{-1} shows distinct ferrite and NdFeB coercivity and saturation values. (b) An 240 kA m^{-1} field switches the ferrite magnetization while leaving the NdFeB unaffected, resulting in a vertically-biased loop intersecting the origin. Traversing the hysteresis loop, the device begins in the "off" state at point "A", where motion actuation fields, indicated by the ±12 kA m^{-1} range, only magnetize the device to about 0.08 μA m^2, resulting in minimal motion actuation. To turn the device on, a 240 kA m^{-1} pulse is applied in the positive y-direction, bringing the device to point "B". After the pulse, the device returns to point "C", in the on state. Here, motion actuation fields vary the device moment between about 1.7 and 1.8 μA m^2. To turn the device off, a negative y-directed pulse is applied, traversing point "D", and returning to the off state at point "A" at the conclusion of the pulse.

3.1 Micropump alignment

When disabling a device by applying a pulse in the backward direction, the antiparallel alignment of the device with respect to the pulse is critical. Even a minor misalignment will result in in-plane torques which would rotate the device into alignment with the pulsed field before the device is disabled. The torques acting on the device during this process are the applied magnetic torque, frictional drag torque and the fluid drag torque. The applied magnetic torque is

$$\vec{T}_m = \mu_0 \vec{m} \times \vec{H}(t), \tag{1}$$

where $\mu_0 = 4\pi \times 10^{-7}\,\mathrm{H\ m^{-1}}$ is the permeability of free space, $\vec{m}$ is the device magnetic moment, and $\vec{H}(t)$ is the applied flux density as a function of time. As the pulse is created by a capacitor bank discharged through a coil (inductor), the applied flux density is governed by the second order series LCR circuit equation[20]

$$\frac{1}{D}\frac{d^2H(t)}{dt^2} + \frac{R}{LD}\frac{dH(t)}{dt} + \frac{1}{LCD}H(t) = 0, \tag{2}$$

where D is the constant relating coil current $i(t)$ to the flux density by $H(t) = Di(t)$ ($D \approx 8.83\,\mathrm{m^{-1}}$ for the pulsing coil used), R is the circuit resistance, L is the circuit inductance and C is the capacitance. The initial condition is given by the initial charge voltage on the capacitor bank V_0 as

$$\left.\frac{dH(t)}{dt}\right|_{t=0} = \frac{V_0}{LD}.$$

The frictional resistive drag torque from contact with the substrate is given as

$$T_f = -\mu_f N \frac{d}{4}, \tag{3}$$

where μ_f is the friction coefficient, N is the normal force (device weight + adhesion), and d is the device diameter. The fluid drag torque, assuming a shear flow between the micropump and the surface, is given as the integral of shear stress τ_d over the micropump area as

$$T_d = \int_A \tau_d r dA = -\frac{\pi \mu d^4 \omega}{32h} \tag{4}$$

where r is the radial distance from the center of the pump, $h = 5\,\mu$m is the estimated micropump-surface space due to surface roughness, μ is the kinematic viscosity of the liquid, and ω is the rotational rate. The total torque from eqns. (1), (3) and (4) is inserted into the single degree of freedom rotational dynamic equation

$$T_m + T_f + T_d = I\frac{d^2\theta}{dt^2}(t) \tag{5}$$

where $I \approx \frac{1}{12}\rho V\left(\frac{d}{2}\right)^2$ is the rotational inertia about the vertical axis and θ is the in-plane rotation angle of the device. An integration of eq. (5) with initial misalignment angle θ_i for the pulse H_{pulse} will determine if the device is disabled before it rotates. This result is shown along with experimental results in Fig. 3(c). The simulation predicts the critical angle range for misalignment tolerance to disable to be $180 \pm 30^\circ$, where $\theta_i = 180^\circ$ denotes the backward (disabling) direction. For larger misalignments (resulting in oblique magnetization), the simulation predictions are erratic due to oscillatory motion. Thus, this regime is not considered in the simulation results.

The critical angle range for misalignment tolerance to disable was found experimentally to be approximately $180 \pm 35^\circ$, as shown in Fig. 3. For initial alignments within $\pm 90^\circ$ of 0° (forward pulses), the device remains magnetized in the forward direction. For moderate misalignments, the device rotates during the pulse and the resulting magnetization is not in the forward direction (and tends to be unpredictable).

As seen in eq. (5), to increase the allowable disabling misalignment, the friction and drag torque can be increased by choice of geometry, material, and fluid properties, the magnetic torque can be decreased by reducing the strength of the magnetic moment m, or the pulse rise time can be shortened to magnetize the device sooner by lowering the circuit time constant $\tau = LC$. A reduced value of τ would necessitate an increase in the charge voltage V_0 to maintain the peak H_{pulse} value.

3.2 Selective micropump actuation

The proposed disabling method for microdevices can be used to selectively disable multiple micropumps. Based on their orientation when the pulse is applied (and independent of position), each micropump will be disabled or remain enabled, as was shown in the previous section. To selectively orient multiple micropumps without experiencing any translational motion before the switching pulse is applied, a four step method is employed, as shown in Fig. 4:

1. Using a uniform upward field, all devices are oriented to the same direction ($+y$-direction).

2. Using two horizontal coils operated in opposition, a horizontal field gradient $\frac{dH_x}{dx}$ is applied. At the center of the coil system, a point of zero field exists, positioned over one of the micropumps. This point can be shifted horizontally to select different devices for disabling.

3. A uniform field in the $-y$-direction is applied, rotating all devices except the selected device, which has zero torque due to being antiparallel to the applied field.

4. The field pulse H_{pulse} is applied to disable all devices pointing in the $+y$-direction. Devices pointing in the $-y$-

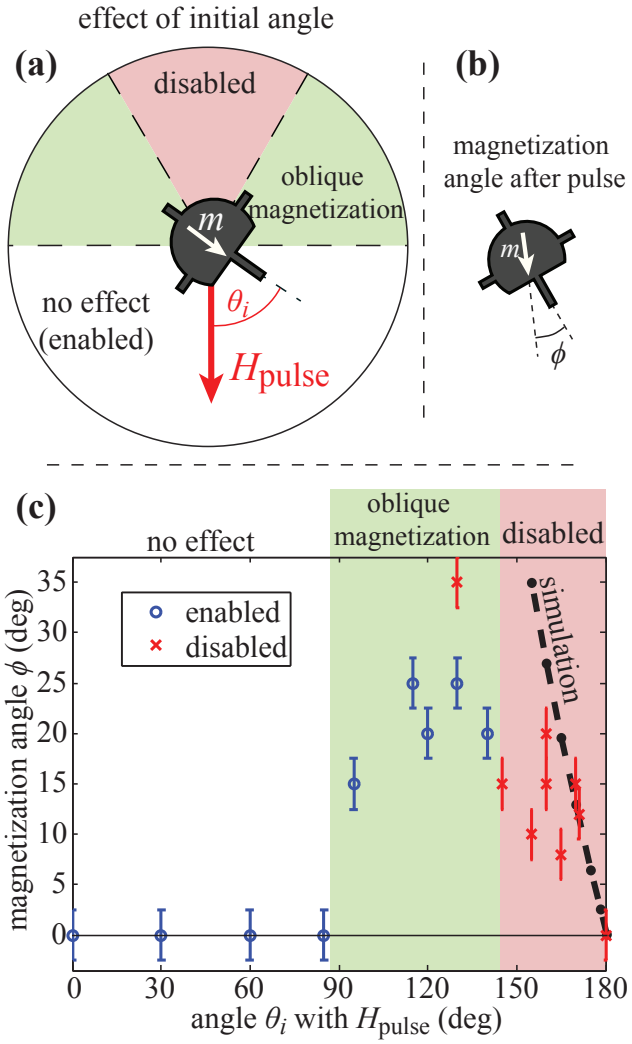

Fig. 3 Permissible initial misalignment of the micropump with respect to the pulse. (a) The device forward direction relative to the pulse direction is given by θ_i. For forward pulses (small θ_i), no change is observed. For moderate misalignment, the micropump resulting magnetization is obliquely oriented. For reverse pulses, the micropump is disabled. (b) The direction of magnetization after the pulse is given by ϕ. (c) The resulting magnetization angle is graphed for various initial misalignment angles. To disable the device, it must be pulsed within $\pm 35°$ of the backward direction. Disabled devices, which are too weak to spin, still retain a small amount of magnetization in the forward direction. The dotted line shows the simulated values of ϕ for small misalignments.

direction are unaffected because their orientation $\theta_i = 0°$ is parallel to H_{pulse} .

Thus, a large number of microdevices can be independently addressed by magnetic disabling if they are adequately spaced in a single direction. The minimum horizontal spacing $s_{\min}$ will depend on the magnitude of the magnetic gradient field created and the minimum torque $T_{\min}$ required to orient the microdevices in step 2 above. Using (1), this minimum spacing can be derived as

$$s_{\min} = \frac{T_{\min}}{\mu_0 m \frac{dH_x}{dx}}. \tag{6}$$

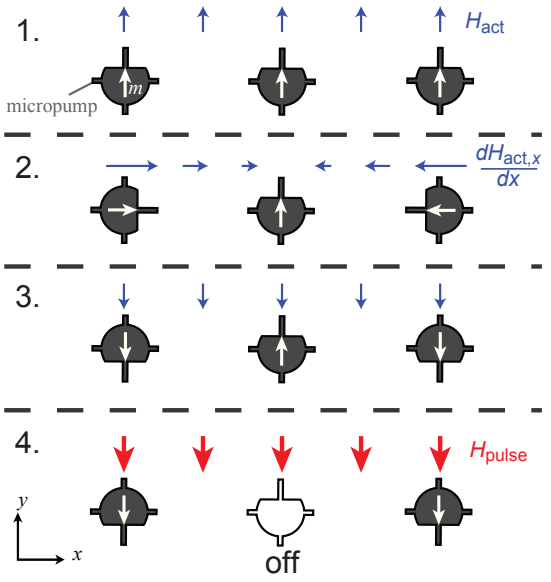

Fig. 4 Selective micropump orientation method. Using a four step process, a single device is chosen to be disabled. 1. Using a uniform upward field, all devices are pointed in the y-direction. 2. Using two horizontal coils operated in opposition, a horizontal field gradient $\frac{dH_x}{dx}$ is applied. At the center of the coil system, a point of zero field exists, positioned over one of the micropumps. This point can be shifted horizontally to select different devices for disabling. 3. A uniform $-y$ field is applied, rotating all devices down except the selected device, which has zero torque due to being antiparallel to the applied field. 4. The switching pulse H_{pulse} is applied to switch all devices pointing in the $+y$-direction. Devices pointing in the $-y$-direction are unaffected. Fluid channels are not shown for clarity.

Multiple pumps can be disabled by repeating the process for each pump to be disabled. Previously disabled pumps will remain oriented in the $+y$-direction while subsequent pumps are disabled. Selective actuation could be achieved for two-dimensional arrays of microdevices through the concurrent use of x- and y-directed field gradients, but is not shown in this work.

3.3 Micropump switching

A $800 \times 800 \times 75\,\mu\text{m}^3$ micropump is tested *in-situ* to characterize the magnetic switching behavior. The simple remote motion actuation task used to test the micropump consists of finding the rotation rate of the micropump in the presence of a 5 Hz rotating magnetic field of magnitude $5.0\,\text{kA m}^{-1}$. The rotation rate is observed visually from experimental video taken at 70 Hz. Each "enabling" experiment begins with the device fully off from $H_{\text{pulse}} = 240\,\text{kA m}^{-1}$ in the backward

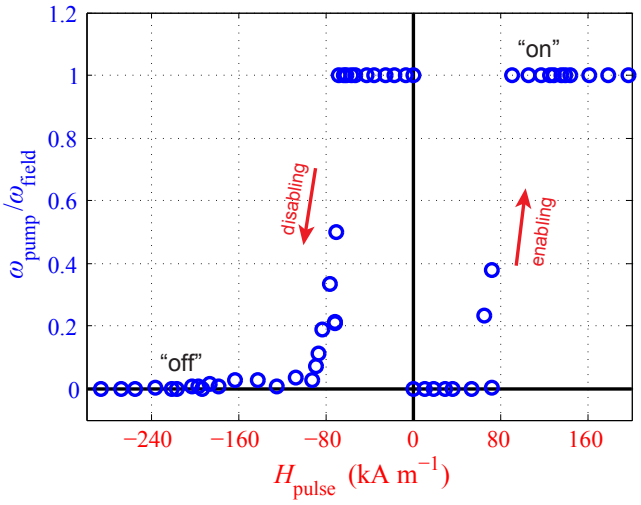

Fig. 5 Micropump motion actuation as a function of pulse strength, showing hysteresis behavior. Motion actuation is taken as the rotation speed of the micropump ω_{pump}, normalized by the rotation speed of the applied field ω_{field}. When being disabled from the on state using negative H_{pulse}, a fully on state is observed for pulses weaker than -70 kA m^{-1} and fully off for pulses stronger than -210 kA m^{-1}. When being enabled from the off state using positive H_{pulse}, a fully off state is observed for pulses less than 60 kA m^{-1} and fully on for pulses greater than 80 kA m^{-1}.

direction. Then H_{pulse} of various strengths is applied in the forward direction to turn on the device. These data points are shown as positive H_{pulse} values in Fig. 5. Each "disabling" experiment begins with the device fully on, with H_{pulse} of various strengths applied in the backward direction to turn off the device. These data points are shown as negative H_{pulse} values in Fig. 5. Motion actuation is taken as the rotation speed of the micropump ω_{pump}, normalized by the rotation speed of the applied field ω_{field}, showing clear micropump "on" and "off" states. It is seen that the device remains fully on with negative pulses weaker than -70 kA m^{-1}, and becomes fully off with pulses stronger than -210 kA m^{-1}. It is seen that the device begins to enable with positive H_{pulse} around 60 kA m^{-1}, and becomes fully on at around H_{pulse} = 90 kA m^{-1}. The sharp change in actuation for a critical H_{pulse} magnitude is advantageous, and shows that the magnetization of the device need not be completely disabled to prevent the microdevice from rotating at full speed.

3.4 Two micropump switching demonstration

Two 800 μm micropumps are placed in polyurethane microchannels similar to those used in conventional microfluidic devices[21] as shown schematically in Fig. 6(a). Polyurethane is used in place of the usual polydimethylsiloxane because polyurethane shows lower adhesion with the micropumps. Each micropump is placed offset in the channel to provide the pumping motion as in Agarwal et. al,[9] and is constrained to its location by a polyurethane post in the center of the offset region. After placement of the micropumps in their channels, a glass cover slip is bonded to the top of the polyurethane to enclose the channels. Light pressure is applied to ensure a close seal between the polyurethane layer and the glass. The entire assembly is then placed in the electromagnetic coil system for actuation.

The flow in each independent channel is visualized by optically tracking small suspended black particles of approximate size 10-50 μm in the 5 cSt silicone oil liquid. The approximate flow rate q is calculated from the fastest particle in each channel by assuming a parabolic velocity distribution in the channel of width 100 μm and height 150 μm. Thus, the mean velocity is taken as approximately half of the maximum velocity,[22] averaged over at least 1.0 sec. The fabricated micropumps are disabled using the methods presented to show addressing of two devices in Fig. 6(b-e), which represents one continuous experiment, and show that any combination of micropump states are achievable. Pumps in the "off" state are not completely disabled, and vibrate slightly without rotating, resulting in minimal fluid motion. The approximate flow rate is shown below each channel in Fig. 6(b-e), showing distinct "on" and "off" states. In Fig. 6(e), a small negative flow rate is seen because all channels are connected at the ends, resulting in some coupling between the flows. This could be avoided through the use of independent channels for each micropump. Variation in flow rate for the "on" micropumps is due to the gap of about 20 μm between the micropump and the post about which it rotates. This means that the pump-wall spacing may vary between trials, which can affect the rate of pumping. This flow rate variation could be reduced by tightening the gap through more precise fabrication. Limited by the video resolution for particle tracking, the flow rates are found with an approximate error of $\pm 0.2 \times 10^{-4}$ ml min^{-1}.

3.5 Five microdevice switching demonstration

To demonstrate the capabilities for scalable microdevice addressability using the methods presented, an array of five simple magnetic microactuators are addressed, as shown in Fig. 7. Here, 600 μm arrow shapes rotate about polyurethane posts on a polyurethane surface in silicone oil of viscosity 20 cSt without the added complexity of the microchannels as a proof-of-concept demonstration.

It is shown in Fig. 7(a-d) that any device can be disabled while all other devices remain on and in Fig. 7(f) that all devices but one can be turned off. In addition, to turn off more than one device, a multi-step method is used starting with a single disabled pump. This disabled pump now maintains its orientation. Then, the second pump to disable is selectively

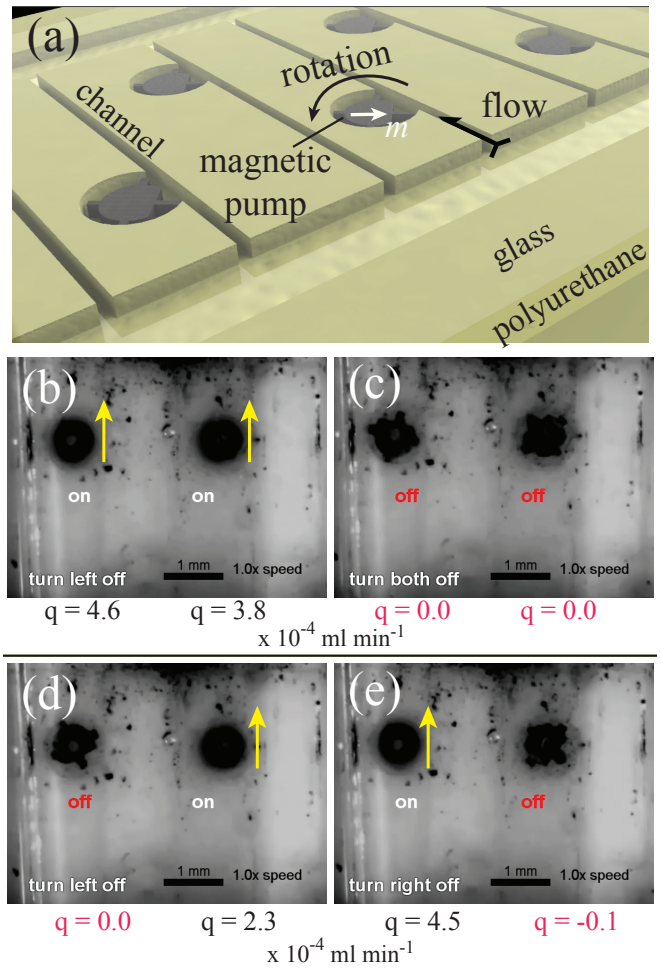

Fig. 6 Frames from a video of two addressable micropumps in microfluidic channels. (a) A rendering of the fluid channel for an array of micropumps. Each of the micropumps, actuated by rotating applied field of magnitude 9.0 kA m^{-1} at a rate of 30 Hz, can be addressed by selective disabling. (b) Both micropumps are on. (c) Both micropumps are off. (d) The left micropump is disabled. (e) The right micropump is disabled. The liquid is 5 cSt silicone oil, and black ink particles are included for flow visualization. Flow direction is indicated by yellow arrow and the approximate flow rate q is given below each channel with an approximate error of $\pm 0.2 \times 10^{-4}$ ml min^{-1}. Video showing selective pumping is available in supplementary materials.

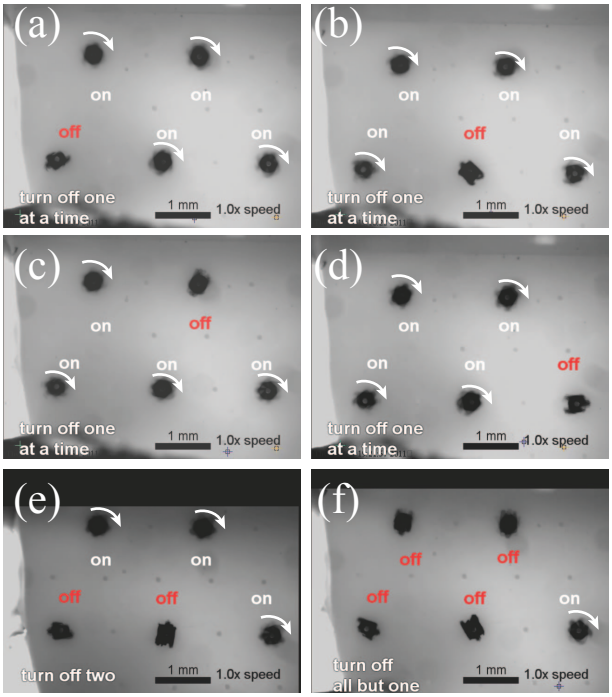

Fig. 7 Frames from a video of five addressable microactuators, spinning in place about a polyurethane post by a rotating applied field of magnitude 4.0 kA m^{-1} at a rate of 30 Hz. Each of the microactuators can be addressed by selective disabling. Rotating actuators are seen as blurry, and are also indicated with rotation arrows. (a-d) One microactuator at a time is turned off. (e) Two microactuators are turned off in sequence. (f) All actuators but one is turned off. Video is available in supplementary materials.

oriented to align with the already disabled pump. At this point, a pulse turns the second device off. In this way, any desired combination of devices can be turned on or off, as seen in Fig. 7(e).

4 Conclusions

We demonstrated a new micro-scale magnetic composite micropump which can be remotely and repeatedly switched between "on" and "off" states by an externally-generated magnetic field pulse. The switching behavior was found to clearly reduce the motion actuation of the device in the "off" state to nearly zero. Through the use of spatial magnetic field gradients, single or multiple micropumps were selected for disabling, leading to addressable pumping behavior for multiple microdevice applications. The scalability of the concept was demonstrated with a simplified microdevice array. Here, five microdevices were individually addressed in any combination.

Although the devices shown are around 800 μm in size, the device is expected to scale smaller without change in performance as long as the magnetic properties are maintained. High viscosity liquid was used in this study to allow for easier disabling, but liquid such as water could be used if the charge voltage of the pulsing circuit is increased to several thousand volts and the capacitance reduced, allowing a faster pulse rise time with the same H_{pulse} peak value. The addressable magnetic composite microdevice concept can be extended to other micro-scale systems using magnetic actuation, and the composite material can be simply molded into any desired shape. Future works will include the use of this switching device as an addressable actuation method for microfluidic valves, mobile microrobots, and other magnetic microelectromechanical

devices.

References

1 K. S. Ryu, K. Shaikh, E. Goluch, Z. Fan and C. Liu, *Lab on a chip*, 2004, **4**, 608–13.

2 K. Ishiyama, M. Sendoh, A. Yamazaki and K. Arai, *Sensors and Actuators A: Physical*, 2001, **91**, 141–144.

3 T. Honda, K. Arai and K. Ishiyama, *IEEE Transactions on Magnetics*, 1996, **32**, 5085–5087.

4 D. R. Frutiger, K. Vollmers, B. E. Kratochvil and B. J. Nelson, *The International Journal of Robotics Research*, 2009, **29**, 613–636.

5 S. Floyd, C. Pawashe and M. Sitti, *The International Journal of Robotics Research*, 2009, **28**, 1077–1094.

6 M. Sitti, *Nature*, 2009, **458**, 1121–1122.

7 J. Judy, *Sensors and Actuators A: Physical*, 1996, **53**, 392–397.

8 T. Sawetzki, S. Rahmouni, C. Bechinger and D. W. M. Marr, *PNAS*, 2008, **105**, 20141–5.

9 A. Agarwal, S. Sridharamurthy and D. Beebe, *Journal of Microelectromechanical Systems*, 2005, **14**, 1409–1421.

10 S. Floyd, E. Diller, C. Pawashe and M. Sitti, *The International Journal of Robotics Research*, 2011, **30**, 1553–1565.

11 B. Donald, C. Levey and I. Paprotny, *Microelectromechanical Systems, Journal of*, 2008, **17**, 789–808.

12 C. Pawashe, S. Floyd and M. Sitti, *Applied Physics Letters*, 2009, **94**, 164108.

13 P. Braillon, 1978, patent 4075589.

14 K. Gilpin, A. Knaian and D. Rus, IEEE International Conference on Robotics and Automation, 2010, pp. 2485–2492.

15 D. J. Laser and J. G. Santiago, *Journal of Micromechanics and Microengineering*, 2004, **14**, R35–R64.

16 E. Diller, C. Pawashe, S. Floyd and M. Sitti, *The International Journal of Robotics Research*, 2011, **30**, 1667–1680.

17 M. Imbaby, K. Jiang and I. Chang, *Journal of Micromechanics and Microengineering*, 2008, **18**, 115018.

18 J. Kim, S. E. Chung, S. Choi, H. Lee, J. Kim and S. Kwon, *Nature Materials*, 2011, 747–752.

19 E. Fullerton, *Journal of Magnetism and Magnetic Materials*, 1999, **200**, 392–404.

20 J. Nilsson and S. Riedel, *Electric Circuits*, Prentice Hall, Eighth edn, 2010.

21 G. M. Whitesides and A. D. Stroock, *Physics Today*, 2001, **54**, 42.

22 S. Turns, *Thermal-Fluid Sciences: An Integrated Approach*, Cambridge University Press, 2006.